Supplementary Material

Reaction-transport model for the study sites

To investigate and quantify the processes controlling distributions of dissolved and particulate species as well as the turnover of C, S, N, and P in the upper 650 cm of Namibian mud belt sediments, the data from St. 12, St. 14 and St. 41 were simulated with a diagenetic reaction-transport model. The model was set up based on the previous models developed for studying biogeochemical cycles in the Peruvian upwelling system (Bohlen et al., 2011; Dale et al., 2016a, 2019) and in the Namibian shelf sediments (Dale et al., 2009) and for studying phosphorus cycling in bioturbated marine sediments (Dale et al., 2016b).

Vertical depth profiles of the dissolved and solid species were simulated using 1-D mass conservation equations (Berner, 1980; Boudreau, 1997):

$$\varphi(x)\cdot\frac{\partial C_i(x,t)}{\partial t}=\frac{\partial\left(\varphi(x)\cdot D(x)\cdot\frac{\partial C_i(x,t)}{\partial x}\right)}{\partial x}-\frac{\partial\left(\varphi(x)\cdot v(x)\cdot C_i(x,t)\right)}{\partial x}+\gamma\cdot\varphi(x)\cdot\alpha_{\mathrm{NO_3^-}\,bac}(x)\cdot\left(C_{\mathrm{NO_3^-}\,bac}(0,t)-C_{\mathrm{NO_3^-}\,bac}(x,t)\right)+\varphi(x)\cdot\Sigma R_{C_i}(x,t) \quad \text{(Eq. S1.1, for St. 14 and St. 41)}$$

where $\gamma = 1$ for $NO_3^-{}_{bac}$ and $\gamma = 0$ for all other solutes.

$$\varphi(x)\cdot\frac{\partial C_i(x,t)}{\partial t}=\frac{\partial\left(\varphi(x)\cdot D(x)\cdot\frac{\partial C_i(x,t)}{\partial x}\right)}{\partial x}-\frac{\partial\left(\varphi(x)\cdot v(x)\cdot C_i(x,t)\right)}{\partial x}+\varphi(x)\cdot\alpha(x)\cdot\left(C_i(0,t)-C_{\mathrm{i}}(x,t)\right)+\varphi(x)\cdot\Sigma R_{C_i}(x,t) \quad \text{(Eq. S1.2, for St. 12)}$$

$$(1-\varphi(x))\cdot\frac{\partial G_j(x,t)}{\partial t}=\frac{\partial\left((1-\varphi(x))\cdot D_b(x)\cdot\frac{\partial G_j(x,t)}{\partial x}\right)}{\partial x}-\frac{\partial\left((1-\varphi(x))\cdot w(x)\cdot G_j(x,t)\right)}{\partial x}+(1-\varphi(x))\cdot\Sigma R_{G_j}(x,t) \quad \text{(Eq. S2)}$$

where x (cm) is sediment depth, t (yr) is time, φ is porosity, D (cm^2 yr^{-1}) is the solute–specific diffusion coefficient in the sediment, D_b (cm^2 yr^{-1}) is the bioturbation coefficient, C_i (µmol cm^{-3} of porewater) is the concentration of solute i, G_j is the content of solid species j (dry weight percent, wt.%), v (cm yr^{-1}) is the net velocity of solutes by burial and compaction in addition to upward fluid flow imposed at the lower boundary of the model, w (cm yr^{-1}) is the burial velocity of solids, α (yr^{-1}) is the (bio)irrigation coefficient, $\alpha_{\mathrm{NO_3^-}\,bac}$ (yr^{-1}) is the coefficient for non-local NO_3^- transport by large sulfur bacteria, $C_i(0,t)$ and $C_{\mathrm{NO_3^-}\,bac}(0,t)$ are the concentrations of solutes and NO_3^- in large sulfur bacteria at the sediment–water interface, respectively, and ΣR_{C_i} and ΣR_{G_j} are the sum of biogeochemical reactions for dissolved and solid species.

Solid and dissolved species and upper boundary conditions are listed in Supplementary Table 1. The model simulates the distributions of 15 dissolved species including O_2, NO_2^-, NO_3^-, SO_4^{2-}, H_2S, CH_4, NH_4^+, DIC, PO_4^{3-}, TA (total alkalinity), Ca^{2+}, Mg^{2+}, Fe^{2+}, H_2 and NO_3^- stored within the large sulfur

oxidizing bacteria, termed biological ($NO_3^-{}_{bac}$). A total of 16 solid species simulated in the model including four fractions of POC of varying reactivity, organic sulfur (S_{org}), particulate organic nitrogen (N_{org}), two iron (oxyhydr)oxide fractions (i.e., highly reactive ($Fe(OH)_{3HR}$) and moderately reactive ($Fe(OH)_{3MR}$), unreactive iron (Fe_U)), pyrite (FeS_2), two pools of phosphorous associated with iron (oxyhydr)oxide (P_{FeHR}, P_{FeMR}), P in authigenic hydroxyapatite formed after polyphosphate breakdown (P_{HAp}), intracellular polyphosphate (P_{poly}), P in fish debris (P_{Fish}) and particulate organic phosphorous (P_{org}).

Constitutive equations describing the depth dependency of transport parameters are provided in Supplementary Table 2. Porosity (φ) was described using an exponential function assuming steady–state compaction including the porosity at the sediment–water interface (φ(0)), the porosity below the depth of compaction (φ(L)) and the porosity depth attenuation coefficient (*px*). Solute–specific diffusion coefficients in sediments (D) were calculated from the temperature–dependent molecular diffusion coefficients in seawater (D_W) (Boudreau, 1997) corrected for salinity and pressure using the modified Weissberg equation (Boudreau, 1997). Under the assumption of steady-state compaction, the velocity of solids (*w*) and the velocity of interstitial fluids (*v*) were calculated as the function of the burial velocity of compacted sediments (w_{acc}) and porosity. Model physical and biogeochemical parameters are listed in Supplementary Tables 3, 4. Biogeochemical reactions are in Supplementary Table 5 and rate expressions are in Supplementary Table 6. Model-derived depth-integrated turnover rates are given in Supplementary Table 7. Modelled benthic fluxes and fluxes at 650 cm are listed in Supplementary Table 8.

$NO_3^-{}_{bac}$ represents a contained pool of NO_3^- within microbial cells and is affected by mixing and burial as if it were a particle with no molecular diffusive transport. $NO_3^-{}_{bac}$ was additionally transported into the sediment assuming a non-local source term $\alpha_{NO_3^-{}_{bac}}$ in units of yr^{-1} (Supplementary Table 2):

$$\alpha_{NO_3^-{}_{bac}}(x) = \alpha_{NO_3^-{}_{bac}}(0) \cdot \exp\left(-\frac{x^2}{2 \cdot xIrr^2}\right) \quad \text{(Eq. S3)}$$

where $\alpha_{NO_3^-{}_{bac}}(0)$ is the coefficient at the sediment surface. The parameter $xIrr$ (cm) defines the depth over which $NO_3^-{}_{bac}$ is transported.

The rate of PO_4^{3-} accumulation and storage as P_{poly} in LSB was defined as (Dale et al., 2016b):

$$R_{26} = k_{26} \cdot PO_4^{3-}/(PO_4^{3-} + C_{eq}) \cdot NO_3^-{}_{bac} \cdot H_2S \quad \text{(Eq. S4)}$$

where k_{26} is a constant that depend on rates of DNRA and $DNRN_2$.

The rate of PO_4^{3-} release to porewater through enzymatic hydrolysis of intracellular P_{poly} by large sulfur bacteria is:

$$R_{27} = k_{27} \cdot P_{poly} \cdot \delta \qquad \text{where } \delta = 1 \text{ for } O_2 \leq 1\ \mu M \text{ and } \delta = 0 \text{ for } O_2 > 1\ \mu M \quad \text{(Eq. S5)}$$

These rates were partly constrained by the measured porewater PO_4^{3-} concentrations, as shown later. Rate expressions are summarized in the Supplementary Information (Supplementary Table 6).

Steady state fluxes of solutes, F_C, and solid species, F_G, at the boundaries were calculated as follows:

$$F_{C_i}(x) = \varphi(x) \cdot \left(v(x) \cdot C_i(x) - D(x) \cdot \frac{\partial C_i(x,t)}{\partial x}\right) \quad \text{(Eq. S6)}$$

$$F_{G_j}(x) = \big(1 - \varphi(x)\big) \cdot \rho_s \cdot w(x) \cdot G_j(x,t) \qquad \text{(Eq. S7)}$$

For upper boundary conditions at the sediment-water interface (x = 0 cm), fixed seawater concentrations are defined for solutes, constant fluxes to the seafloor for solids and a fixed NO_3^- concentration for nitrate stored in bacteria which was calculated from the measured biovolume and internal NO_3^- of giant sulfur bacteria at each site (Zabel et al., 2019). The model was solved with a zero-gradient condition for dissolved and solid species at the lower boundary (x = 650 cm) except for H_2S and NH_4^+ at St. 12 (Supplementary Table 1). The spatial derivatives of the coupled partial differential equations were approximated using finite differences and solved using the method-of-lines (Boudreau, 1997) using the ordinary differential equation solver (NDSolve) in MATHEMATICA v. 11.3. All simulations were run to steady state using a grid spacing which increased from 0.0025 cm at the sediment surface to 2.5 cm at depth. Mass conservation was typically better than 99.5%.

Supplementary Tables

Supplementary Table 1. Chemical species included in the model with upper boundary conditions at the sediment-water interface. At the lower boundary, a zero-gradient Neumann boundary was imposed for all species, except for H_2S and NH_4^+ at St. 12 that given at the bottom of the table.

Variable	St. 12, 23°S	St. 14, 23°S	St. 41, 25°S
Solutes (mM)			
Oxygen (O_2)	5.00×10^{-2}	2.63×10^{-2}	5.26×10^{-2}
Nitrate (NO_3^-)	2.44×10^{-2}	2.38×10^{-2}	2.34×10^{-2}
Nitrite (NO_2^-)	1.20×10^{-4}	4.20×10^{-4}	2.02×10^{-4}
Sulfate (SO_4^{2-})	29	29.2	28
Ferrous iron (Fe^{2+})	0	0	0
Ammonium (NH_4^+)	0	1.03×10^{-3}	0
Phosphate (PO_4^{3-})	1.50×10^{-3}	1.30×10^{-3}	9.31×10^{-4}
Dissolved inorganic carbon (DIC)	2.72	2.72	2.72
Hydrogen sulfide (H_2S)	0	0	0
Methane (CH_4)	0	0	0
Total alkalinity (TA)	2.33	2.33	2.33
Calcium (Ca)	10.67	10.36	10.2
Magnesium (Mg)	52	51.49	54.0
Nitrate stored in bacteria ($NO_{3\,bac}^-$) [a]	-	0.18	0.61
Hydrogen (H_2)	0	0	0
Solids (g cm^{-2} yr^{-1})			
Particulate organic carbon (POC_1)	5.46×10^{-4}	6.54×10^{-4}	1.44×10^{-3}
Particulate organic carbon (POC_2)	1.09×10^{-3}	1.96×10^{-3}	2.53×10^{-3}
Particulate organic carbon (POC_3)	2.19×10^{-3}	1.31×10^{-3}	1.8×10^{-4}
Particulate organic carbon (POC_4)	3.82×10^{-3}	0	1.44×10^{-3}
Highly reactive Fe oxide ($Fe(OH)_{3HR}$)	7.28×10^{-6}	5.51×10^{-5}	3.03×10^{-5}
Moderately reactive Fe oxide ($Fe(OH)_{3MR}$)	2.19×10^{-5}	1.83×10^{-7}	3.61×10^{-6}
Unreactive iron (Fe_U)	3.17×10^{-4}	1.04×10^{-4}	1.71×10^{-4}
Pyrite (FeS_2)	0	0	0
$Fe(OH)_{3HR}$ associated P (P_{FeHR})	1.62×10^{-7}	1.22×10^{-6}	6.73×10^{-7}
$Fe(OH)_{3MR}$ associated P(P_{FeMR})	0	0	0
Authigenic carbonate-containing apatite (P_{HAp})	0	0	0
Intracellular polyphosphate (P_{poly})	0	0	0
Particulate organic sulfur (S_{org})	6.01×10^{-4}	2.94×10^{-4}	3.97×10^{-4}
Phosphorus in fish debris (P_{Fish})	4.03×10^{-4}	4.84×10^{-4}	3.77×10^{-4}
Particulate organic phosphorus (P_{org})	4.03×10^{-5}	1.53×10^{-4}	2.18×10^{-4}
Particulate organic nitrogen (N_{org})	1.13×10^{-3}	5.68×10^{-4}	7.83×10^{-4}
Lower boundary (µmol cm^{-3} cm^{-1})			
Ammonium (NH_4^+)	$\partial NH_4^+/_{dx} = -1.00 \times 10^{-3}$	-	-
Hydrogen sulfide (H_2S)	$\partial H_2S/_{dx} = -5.40 \times 10^{-3}$	-	-

[a] Mean of all sampling stations at 23 ºS and 25 ºS where *Thiomargarita* were observed.

Supplementary Table 2. Depth–dependent constitutive equations.

Parameter	Equation
Porosity	$\varphi(x) = \varphi(L) + \big(\varphi(0) - \varphi(L)\big) \cdot \exp(-px \cdot x)$
Diffusion coefficients	$D(x) = \frac{D_W}{1 - \ln(\varphi(x)^2)}$
Burial velocity of solids	$\omega(x) = \frac{\big(1 - \varphi(L)\big) \cdot \omega_{acc}}{\big(1 - \varphi(x)\big)}$
Burial velocity of solutes	$v(x) = \frac{\varphi(L) \cdot \omega_{acc}}{\varphi(x)}$
Bioturbation for all solids	$D_b(x) = D_b(0) \cdot \exp\left(-\frac{x^2}{2 \cdot xBio^2}\right)$
(Bio)irrigation for solutes	$\alpha(x) = \alpha(0) \cdot \exp\left(-\frac{x^2}{2 \cdot xBIB^2}\right)$
Bioirrigation for $NO_3^-{}_{bac}$	$\alpha_{NO_3^-{}_{bac}}(x) = \alpha_{NO_3^-{}_{bac}}(0) \cdot \exp\left(-\frac{x^2}{2 \cdot xlrr^2}\right)$

Supplementary Table 3. Physical parameters used in the model.

Parameter	Description	St. 12, 23°S	St. 14, 23°S	St. 41, 25°S	Unit	Source[a]
L	Length of simulated sediment column	650	650	650	cm	C
T	Bottom water temperature	11.72	11.67	12	°C	M
S	Bottom water salinity	35.05	35.05	35.50	-	M
P	Pressure at seafloor	16.04	14.94	14.84	bar	M
ω_{acc}	Sediment accumulation rate	0.095	0.22	0.11	cm yr^{-1}	M
ρ_s	Dry sediment density	2.5	2.5	2.5	g cm^{-3}	L[1]
$\varphi(0)$	Porosity at 0 cm	0.94	0.98	0.97	-	M
$\varphi(L)$	Porosity at L cm	0.77	0.94	0.87	-	M
px	Parameter for exponential decrease in porosity with depth	1/90	1/15	1/60	1/cm	C
$D_B(0)$	Bioturbation coefficient at sediment surface	83	23.7	35.4	cm^2 yr^{-1}	C
$xBio$	Depth of bioturbated zone	2.6	5.9	7.1	cm	C
$\alpha(0)$	Bio-irrigation coefficient at sediment surface for solutes	50 except Fe^{2+} (=0)	-	-	yr^{-1}	C
$xBIB$	Depth of bio-irrigated zone for solutes	18	-	-	cm	C
$\alpha_{NO_{3\,bac}^-}(0)$	Bio-irrigation coefficient at sediment surface for $NO_{3\,bac}^-$	-	300	100	yr^{-1}	C
$xIrr$	Depth of bio-irrigated zone for $NO_{3\,bac}^-$	-	6	5	cm	C
$D_{SO_4^{2-}}$	Diffusion coefficient for SO_4^{2-}	240	239	242	cm^2 yr^{-1}	L[2]
D_{CH_4}	Diffusion coefficient for CH_4	361	361	364	cm^2 yr^{-1}	L[2]
$D_{NH_4^+}$	Diffusion coefficient for NH_4^+	453	452	456	cm^2 yr^{-1}	L[2]
D_{DIC}	Diffusion coefficient for DIC	261	261	264	cm^2 yr^{-1}	L[2]
D_{H_2S}	Diffusion coefficient for H_2S	403	402	406	cm^2 yr^{-1}	L[2]
$D_{PO_4^{3-}}$	Diffusion coefficient for PO_4^{3-}	168	168	170	cm^2 yr^{-1}	L[2]
$D_{Fe^{2+}}$	Diffusion coefficient for Fe^{2+}	151	150	152	cm^2 yr^{-1}	L[2]
D_{O_2}	Diffusion coefficient for O_2	433	432	436	cm^2 yr^{-1}	L[2]
$D_{NO_3^-}$	Diffusion coefficient for NO_3^-	443	443	447	cm^2 yr^{-1}	L[2]
$D_{NO_2^-}$	Diffusion coefficient for NO_2^-	420	420	423	cm^2 yr^{-1}	L[2]
D_{TA}	Diffusion coefficient for TA	261	261	264	cm^2 yr^{-1}	L[2]
D_{Ca}	Diffusion coefficient for Ca^{2+}	180	180	181	cm^2 yr^{-1}	L[2]
D_{Mg}	Diffusion coefficient for Mg^{2+}	162	161	163	cm^2 yr^{-1}	L[2]
$D_{NO_{3\,bac}^-}$	Diffusion coefficient for $NO_{3\,bac}^-$	-	1	1	cm^2 yr^{-1}	C
D_{H_2}	Diffusion coefficient for H_2	605	605	605	cm^2 yr^{-1}	L[2]

[a] Parameter values were based on the following sources: C. Constrained with the model. M. Measured. L. Assumed value from literature: [1]Dale et al. (2006b); [2]Boudreau et al. (1997).

Supplementary Table 4. Biogeochemical parameters used in the model.

Parameter	Description	St. 12, 23°S	St. 14, 23°S	St. 41, 25°S	Unit	Source[a] (St. 12; St. 14; St. 41)
k_{POC1}	First order kinetic constant for POC1 degradation	32.9	30	11.9	yr^{-1}	C; C; C
k_{POC2}	First order kinetic constant for POC2 degradation	1.65×10^{-2}	5.07×10^{-3}	8.87×10^{-3}	yr^{-1}	C; C; C
k_{POC3}	First order kinetic constant for POC3 degradation	5.27×10^{-3}	7.39×10^{-5}	1.10×10^{-3}	yr^{-1}	C; C; C
k_{POC4}	First order kinetic constant for POC4 degradation	0	0	0	yr^{-1}	C; C; C
k_7	Rate constant for aerobic oxidation of NO_2^-	1×10^{7}	1×10^{4}	1×10^{4}	$mM^{-1}\ yr^{-1}$	L; C; C
k_8	Rate constant for aerobic oxidation of Fe^{2+}	1×10^{6}	1×10^{5}	1×10^{5}	$mM^{-1}\ yr^{-1}$	C; C; C
k_9	Rate constant for aerobic oxidation of FeS_2	1×10^{2}	1×10^{3}	1×10^{3}	$mM^{-1}\ yr^{-1}$	C; L; L
k_{10}	Rate constant for aerobic oxidation of H_2S	1×10^{5}	1×10^{3}	1×10^{3}	$mM^{-1}\ yr^{-1}$	L; C; C
k_{11}	Rate constant for aerobic oxidation of CH_4	1×10^{-10}	1×10^{-10}	1×10^{-10}	$mM^{-1}\ yr^{-1}$	C; C; C
k_{12}	Rate constant for aerobic oxidation of NH_4^+	1×10^{7}	1×10^{4}	1×10^{4}	$mM^{-1}\ yr^{-1}$	L; C; C
k_{13}	Rate constant for anaerobic oxidation of Fe^{2+}	1×10^{7}	1×10^{6}	1×10^{6}	$mM^{-1}\ yr^{-1}$	L; C; C
k_{14}	Rate constant for anaerobic oxidation of Fe^{2+}	1×10^{7}	1×10^{6}	1×10^{6}	$mM^{-1}\ yr^{-1}$	C; C; C
k_{15}	Rate constant for anaerobic oxidation of H_2S (DNRA) by giant sulfur bacteria	0	1.8×10^{5}	4×10^{3}	$mM^{-1}\ yr^{-1}$	C; C; C
k_{16}	Rate constant for anaerobic oxidation of H_2S ($DNRN_2$) by giant sulfur bacteria	0	6.864×10^{5}	1.3×10^{4}	$mM^{-1}\ yr^{-1}$	C; C; C
k_{17}	Rate constant for anaerobic oxidation of H_2S	0	0	0	$mM^{-1}\ yr^{-1}$	C; C; C
k_{18}	Rate constant for anammox	1×10^{9}	1×10^{5}	1×10^{5}	$mM^{-1}\ yr^{-1}$	C; C; C
k_{19}	Rate constant for anaerobic oxidation of CH_4	200	200	200	$mM^{-1}\ yr^{-1}$	C; C; C
k_{20}	Rate constant for FeS_2 precipitation	2000	1000	500	$mM^{-1}\ yr^{-1}$	C; C; C
k_{21}	Rate constant for $Fe(OH)_{3HR}$ / $Fe(OH)_{3MR}$ reduction by H_2S	1 / 0.5	100 / 1	10 / 0.01	$mM^{-1}\ yr^{-1}$	C; C; C
k_{22}	Rate constant for $Fe(OH)_{3HR}$ ageing to $Fe(OH)_{3MR}$	0.8	15	40	yr^{-1}	C; C; C
k_{23}	Rate constant for precipitation of P_{HAp}	0.005	1.25	3.41	yr^{-1}	C; C; C
k_{24}	Rate constant for calcium carbonate precipitation	0.5	0.5	0.5	yr^{-1}	C; C; C
k_{25}	Rate constant for magnesium carbonate precipitation	0.5	0.5	0.5	yr^{-1}	C; C; C
k_{26}	Rate constant for polyphosphate synthesis[b]	0	0.9	0.06	$mM^{-1}\ yr^{-1}$	C; C; C
k_{27}	Rate constant for polyphosphate breakdown	0	15	0.02	yr^{-1}	C; C; C
k_{28}	Rate constant for sulfidization of organic matter	0.0002	0.0002	0.0002	$mM^{-1}\ yr^{-1}$	C; C; C
k_{29}	Rate constant for decomposition of phosphorous in fish debris	0.05	6	0.9	yr^{-1}	C; C; C
k_{30}	Rate constant for sulfate reduction by H_2	1×10^{6}	1×10^{6}	1×10^{6}	$mM^{-1}\ yr^{-1}$	C; C; C
K_{O2}	Half–saturation constant for O_2 for OM degradation	0.01	0.01	0.01	mM	C; C; C
K_{NO3}	Half–saturation constant for NO_3^- for OM degradation	0.005	0.005	0.005	mM	C; C; C
K_{NO2}	Half–saturation constant for NO_2^- for OM degradation	0.0005	0.005	0.005	mM	C; C; C
K_{Fe}	Half–saturation constant for $Fe(OH)_{3HR}$ for OM degradation	0.0001	0.0001	0.0001	gFe /g	C; C; C
K_{SO4}	Half–saturation constant for SO_4^{2-} for OM degradation	0.1	0.1	0.1	mM	C; C; C
K_{PO4}	Half–saturation constant for PO_4^{3-} uptake into $Fe(OH)_{3HR}$	0.01	0.01	0.01	mM	L; L; L
ε_{aut}	Fe:P ratio in authigenic $Fe(OH)_{3HR}$	10	10	10	mol Fe $(mol\ P)^{-1}$	L; L; L
ε_{age}	Fe:P ratio in $Fe(OH)_{3MR}$ recrystallized from $Fe(OH)_{3HR}$	40	40	40	mol Fe $(mol\ P)^{-1}$	L; L; L
ε_{allHR}	Fe:P ratio in deposited $Fe(OH)_{3HR}$	25	25	25	mol Fe $(mol\ P)^{-1}$	L; L; L
ε_{allMR}	Fe:P ratio in deposited $Fe(OH)_{3MR}$	0	0	0	mol Fe $(mol\ P)^{-1}$	L; L; L

C_{eq}	Equilibrium PO_4^{3-} concentration for P_{HAp} precipitation	0.0001	0.04	0.03	mM	C; C; C
r_{PC1}	Atomic P-C ratio in deposited organic matter	0.03/106	1.6/106	1.6/106	mol P (mol C)$^{-1}$	C; C; C
r_{PC2}	Atomic P-C ratio in deposited organic matter	0.5/106	1.6/106	1.6/106	mol P (mol C)$^{-1}$	C; C; C
r_{PC3}	Atomic P-C ratio in deposited organic matter	0.5/106	1.6/106	1.6/106	mol P (mol C)$^{-1}$	C; C; C
r_{PC4}	Atomic P-C ratio in deposited organic matter	0	0	1.6/106	mol P (mol C)$^{-1}$	C; C; C
r_{PCr1}	Atomic P-C remineralization ratio	0.25/106	8.9/106	5.55/106	mol P (mol C)$^{-1}$	C; C; C
r_{PCr2}	Atomic P-C remineralization ratio	0.4/106	0.03/106	0.3/106	mol P (mol C)$^{-1}$	C; C; C
r_{PCr3}	Atomic P-C remineralization ratio	0.4/106	0.03/106	0.2/106	mol P (mol C)$^{-1}$	C; C; C
r_{PCr4}	Atomic P-C remineralization ratio	-	-	-	mol P (mol C)$^{-1}$	C; C; C
r_{NC}	Atomic N-C ratio in deposited organic matter	0.127	0.124	0.12	mol N (mol C)$^{-1}$	C; C; C
r_{NCr}	Atomic N-C remineralization ratio	0.18	0.13	0.12	mol N (mol C)$^{-1}$	C; C; C

[a] Parameter values were based on the following sources: C. Constrained with the model. L. Assumed value from literature (Dale et al., 2016b).
[b] k_{26} depends on rates of DNRA and $DNRN_2$ (i.e., $k_{26}= f_{26}\cdot(k_{15} + k_{16})$. f_{26} is the factor for polyphosphate synthesis depending on rates of DNRA and $DNRN_2$. f_{26} = 0.9 at St. 14 and f_{26} = 0.06 at St. 41.

Supplementary Table 5. Reactions considered in the biogeochemical model that includes the microbial P pump.

Reaction	Description	Stoichiometry	Footnote
		Organic matter mineralization reactions (Primary redox reactions)	
R_1	Aerobic POM degradation	$CNr_{NCr}Pr_{PCr} + O_2 \rightarrow TCO_2 + r_{NCr}NH_4^+ + r_{PCr}PO_4^{3-}$	
R_2	POM degradation coupled to nitrate reduction	$CNr_{NCr}Pr_{PCr} + 2NO_3^- \rightarrow 2NO_2^- + TCO_2 + r_{NrC}NH_4^+ + r_{PCr}PO_4^{3-}$	
R_3	POM degradation coupled to nitrite reduction	$CNr_{NCr}Pr_{PCr} + 1.33NO_2^- \rightarrow 0.66N_2 + TCO_2 + r_{NCr}NH_4^+ + r_{PCr}PO_4^{3-}$	
R_4	POM degradation coupled to iron reduction	$CNr_{NCr}Pr_{PCr} + 4Fe(OH)_{3HR} + 4\theta_{HR}P_{FeHR} \rightarrow 4Fe^{2+} + TCO_2 + r_{NCr}NH_4^+ + (4\theta_{HR} + r_{PCr})PO_4^{3-}$	a
R_5	POM degradation coupled to sulfate reduction	$CNr_{NCr}Pr_{PCr} + 0.5SO_4^{2-} \rightarrow 0.5H_2S + TCO_2 + r_{NCr}NH_4^+ + r_{PCr}PO_4^{3-}$	
R_6	POM degradation coupled to methanogenesis	$CNr_{NCr}Pr_{PCr} \rightarrow 0.5CH_4 + 0.5TCO_2 + r_{NCr}NH_4^+ + r_{PCr}PO_4^{3-}$	
		Secondary redox reactions	
R_7	Aerobic NO_2^- oxidation	$NO_2^- + 0.5O_2 \rightarrow NO_3^-$	
R_8	Aerobic Fe^{2+} oxidation	$Fe^{2+} + 0.25O_2 + 1/\varepsilon_{aut}\cdot PO_4^{3-} + 2.5H_2O \rightarrow Fe(OH)_{3HR} + 1/\varepsilon_{aut}\cdot PFe_{HR} + 2H^+$	b
R_9	Aerobic FeS_2 oxidation	$FeS_2 + 3.5O_2 + H_2O \rightarrow Fe^{2+} + 2SO_4^{2-} + 2H^+$	
R_{10}	Aerobic H_2S oxidation	$H_2S + 2O_2 \rightarrow SO_4^{2-} + 2H^+$	
R_{11}	Aerobic CH_4 oxidation	$CH_4 + 2O_2 \rightarrow TCO_2 + 2H_2O$	
R_{12}	Aerobic NH_4^+ oxidation	$NH_4^+ + 1.5O_2 \rightarrow NO_2^- + 2H^+ + H_2O$	
R_{13}	Anaerobic Fe^{2+} oxidation with NO_2^-	$Fe^{2+} + 1/3NO_2^- + 1/\varepsilon_{aut}\cdot PO_4^{3-} + 7/3H_2O \rightarrow 1/6N_2 + Fe(OH)_{3HR} + 1/\varepsilon_{aut}\cdot P_{FeHR} + 5/3H^+$	
R_{14}	Anaerobic Fe^{2+} oxidation with NO_3^-	$Fe^{2+} + 0.2NO_3^- + 1/\varepsilon_{aut}\cdot PO_4^{3-} + 12/5H_2O \rightarrow 0.1N_2 + Fe(OH)_{3HR} + 1/\varepsilon_{aut}\cdot P_{FeHR} + 9/5H^+$	
R_{15}	Dissimilatory nitrate reduction to ammonium (DNRA)	$H_2S + NO_{3\ bac}^- + H_2O \rightarrow SO_4^{2-} + NH_4^+$	d
R_{16}	Chemolithotrophic denitrification ($DNRN_2$)	$5/8H_2S + NO_{3\ bac}^- \rightarrow 0.5N_2 + 0.5H_2O + 5/8SO_4^{2-} + 0.25H^+$	d
R_{17}	Anaerobic H_2S oxidation with NO_2^-	$3/8H_2S + NO_2^- + 0.25H^+ \rightarrow 3/8SO_4^{2-} + 0.5H_2O + 0.5N_2$	
R_{18}	Anaerobic NH_4^+ oxidation (anammox)	$NH_4^+ + NO_2^- \rightarrow N_2 + 2H_2O$	
R_{19}	Anaerobic CH_4 oxidation with SO_4^{2-} (AOM)	$CH_4 + SO_4^{2-} + 2H^+ \rightarrow H_2S + TCO_2 + 2H_2O$	
R_{20}	FeS_2 precipitation	$\Sigma\ Fe^{2+} + 2H_2S \rightarrow FeS_2 + H_2 + 2H^+$	
R_{21}	Iron (oxyhydr)oxide reduction by H_2S	$\Sigma\ Fe(OH)_{3j} + \theta_j P_{Fej} + H_2S + H^+ \rightarrow 0.5FeS_2 + \theta_j PO_4^{3-} + 0.5Fe^{2+} + 3H_2O$	a, c
R_{22}	$Fe(OH)_{3HR}$ aging to $Fe(OH)_{3MR}$	$Fe(OH)_{3HR} + \theta_{HR}P_{FeHR} + 1/\varepsilon_{age}\cdot PO_4^{3-} \rightarrow Fe(OH)_{3MR} + \theta_{HR}PO_4^{3-} + 1/\varepsilon_{age}\cdot P_{FeMR}$	a
R_{23}	Authigenic hydroxyapatite precipitation	$5Ca^{2+} + 3PO_4^{3-} + H_2O \rightarrow Ca_5(PO_4)_3(OH) + H^+$	
R_{24}	Calcium carbonate precipitation	$Ca^{2+} + CO_3^{2-} \rightarrow CaCO_3$	
R_{25}	Magnesium carbonate precipitation	$Mg^{2+} + CO_3^{2-} \rightarrow MgCO_3$	
R_{26}	Polyphosphate accumulation	$PO_4^{3-} \rightarrow P_{poly}$	d
R_{27}	Polyphosphate breakdown	$P_{poly} \rightarrow PO_4^{3-}$	d
R_{28}	Sulfidization of POC	$(POC_1+POC_2)+H_2S \rightarrow$"POC-$H_2S$"	
R_{29}	Fish debris dissolution	$P_{Fish} \rightarrow PO_4^{3-}$	
R_{30}	Sulfate reduction with H_2	$0.25SO_4^{2-} + H_2 + 0.5H^+ \rightarrow 0.25H_2S + H_2O$	

[a] Moles of iron-associated P released from iron oxide dissolution (R_5 and R_{26}) and ageing (R_{28}) is calculated (per mole of iron reacted) as $\theta_j = \frac{P_{Fej}\cdot f_{Fe}}{Fe(OH)_{3j}\cdot f_P}$, where the unit conversion factor f_{Fe} and f_P are defined in footnote b in Supplementary Table 6.

[b] For j = HR and MR.

[c] Dissolution by sulfide applies to j = HR and MR, whereas Fe-associated P applies to j = HR and MR.

[d] At St. 12, R_{15}, R_{16}, R_{26} and R_{27} were not included since no LSB were observed.

Supplementary Table 6. Rate expressions and units for the model including the microbial P pump. Separate expressions are given in gray for iron-associated P uptake and release.

Rate	Rate expression [a]	Unit [b,c]
R_{POC}	$k_{POC1} \cdot POC_1 + k_{POC2} \cdot POC_2 + k_{POC3} \cdot POC_3 + k_{POC4} \cdot POC_4$	µmol C cm^{-3} yr^{-1}
R_{NH_4POC}	$r_{NCr} \cdot RPOC$	µmol N cm^{-3} yr^{-1}
R_{PO_4POC}	$r_{PCr1} \cdot k_{POC1} \cdot POC_1 + r_{PC2} \cdot k_{POC2} \cdot POC_2 + r_{PC3} \cdot k_{POC3} \cdot POC_3 + r_{PC4} \cdot k_{POC4} \cdot POC_4$	µmol P cm^{-3} yr^{-1}
R_1	$R_{POC} \cdot f_{K-O_2}$	µmol C cm^{-3} yr^{-1}
R_{1PO_4POC}	$R_{PO4POC} \cdot f_{K-O_2}$	µmol P cm^{-3} yr^{-1}
R_2	$R_{POC} \cdot f_{K-NO_3} \cdot \prod_{j=O_2,NO_2}(1 - f_{K-j})$	µmol N cm^{-3} yr^{-1}
R_{2PO_4POC}	$R_{PO4POC} \cdot f_{K-NO_3} \cdot \prod_{i=O_2,NO_2}(1 - f_{K-j})$	µmol P cm^{-3} yr^{-1}
R_3	$R_{POC} \cdot f_{K-NO_2} \cdot \prod_{j=O_2}(1 - f_{K-j})$	µmol N cm^{-3} yr^{-1}
R_{3PO_4POC}	$R_{PO4POC} \cdot f_{K-NO_2} \cdot \prod_{i=O_2}(1 - f_{K-j})$	µmol P cm^{-3} yr^{-1}
R_4	$R_{POC} \cdot f_{K-Fe(OH)_{3HR}} \cdot \prod_{j=O_2,NO_2,NO_3}(1 - f_{K-j})$	µmol Fe cm^{-3} yr^{-1}
R_{4PO_4POC}	$R_{PO4POC} \cdot f_{K-Fe(OH)_{3HR}} \cdot \prod_{j=O_2,NO_2,NO_3}(1 - f_{K-j})$	µmol P cm^{-3} yr^{-1}
$R_{4P_{Fe}}$	$(4\theta_{HR} \cdot R_{POC}) \cdot f_{K-Fe(OH)_{3HR}} \cdot \prod_{j=O_2,NO_2,NO_3}(1 - f_{K-j})$	µmol P cm^{-3} yr^{-1}
R_5	$R_{POC} \cdot f_{K-SO_4} \cdot \prod_{j=O_2,NO_2,NO_3,Fe(OH)_{3HR}}(1 - f_{K-j})$	µmol S cm^{-3} yr^{-1}
R_{5PO_4POC}	$R_{PO4POC} \cdot f_{K-SO_4} \cdot \prod_{j=O_2,NO_2,NO_3,Fe(OH)_{3HR}}(1 - f_{K-j})$	µmol P cm^{-3} yr^{-1}
R_6	$R_{POC} \cdot \prod_{j=O_2,NO_2,NO_3,Fe(OH)_{3HR},SO_4}(1 - f_{K-j})$	µmol CH_4 cm^{-3} yr^{-1}
R_{6PO_4POC}	$R_{PO4POC} \cdot \prod_{j=O_2,NO_2,NO_3,Fe(OH)_{3HR},SO_4}(1 - f_{K-j})$	µmol P cm^{-3} yr^{-1}
R_7	$k_7 \cdot O_2 \cdot NO_2^-$	µmol N cm^{-3} yr^{-1}
R_8	$k_8 \cdot O_2 \cdot Fe^{2+}$	µmol Fe cm^{-3} yr^{-1}
$R_{8P_{Fe}}$	$\varepsilon_{aut}^{-1} \cdot k_8 \cdot O_2 \cdot Fe^{2+} \cdot f_{K\text{-}PO4}$	µmol P cm^{-3} yr^{-1}
R_9	$k_9 \cdot O_2 \cdot FeS_2$	µmol Fe cm^{-3} yr^{-1}
R_{10}	$k_{10} \cdot O_2 \cdot H_2S$	µmol S cm^{-3} yr^{-1}
R_{11}	$k_{11} \cdot O_2 \cdot CH_4$	µmol C cm^{-3} yr^{-1}
R_{12}	$k_{12} \cdot O_2 \cdot NH_4^+$	µmol N cm^{-3} yr^{-1}
R_{13}	$k_{13} \cdot Fe^{2+} \cdot NO_2^-$	µmol Fe cm^{-3} yr^{-1}
$R_{13P_{Fe}}$	$\varepsilon_{aut}^{-1} \cdot k_{13} \cdot NO_2^- \cdot Fe^{2+} \cdot f_{K\text{-}PO4}$	µmol P cm^{-3} yr^{-1}
R_{14}	$k_{14} \cdot NO_3^- \cdot Fe^{2+}$	µmol Fe cm^{-3} yr^{-1}
$R_{14P_{Fe}}$	$\varepsilon_{aut}^{-1} \cdot k_{14} \cdot NO_3^- \cdot Fe^{2+} \cdot f_{K\text{-}PO4}$	µmol P cm^{-3} yr^{-1}
R_{15}	$k_{15} \cdot NO_{3\,bac}^- \cdot H_2S$	µmol N cm^{-3} yr^{-1}
R_{16}	$k_{16} \cdot NO_{3\,bac}^- \cdot H_2S$	µmol N cm^{-3} yr^{-1}
R_{17}	$k_{17} \cdot NO_2^- \cdot H_2S$	µmol N cm^{-3} yr^{-1}
R_{18}	$k_{18} \cdot NO_2^- \cdot NH_4^+$	µmol N_2 cm^{-3} yr^{-1}
R_{19}	$k_{19} \cdot CH_4 \cdot SO_4^{2-}$	µmol C cm^{-3} yr^{-1}
R_{20}	$k_{20} \cdot Fe^{2+} \cdot H_2S$	µmol Fe cm^{-3} yr^{-1}
R_{21}	$k_{21} \cdot Fe(OH)_{3j} \cdot H_2S$ (for j = HR, MR, PR)	µmol Fe cm^{-3} yr^{-1}
$R_{21P_{Fe}(HR/MR)}$	$\theta_j \cdot k_{21} \cdot Fe(OH)_{3j} \cdot TH_2S$ (for j = HR, MR)	µmol P cm^{-3} yr^{-1}
R_{22}	$k_{22} \cdot Fe(OH)_{3HR}$	µmol Fe cm^{-3} yr^{-1}
$R_{22P_{Fe}}$	$\theta_{HR} \cdot k_{22} \cdot Fe(OH)_{3HR} - 1/\varepsilon_{age} \cdot k_{22} \cdot Fe(OH)_{3HR}$	µmol P cm^{-3} yr^{-1}
R_{23}	$k_{23} \cdot (PO_4^{3-} - C_{eq}) \cdot (0.5+0.5 \cdot erf((PO_4^{3-} - C_{eq})\text{-}0)/10^{-5})$	µmol P cm^{-3} yr^{-1}
R_{24}	$k_{24} \cdot (Ca - Ca_{(OBS)})$	µmol Ca cm^{-3} yr^{-1}
R_{25}	$k_{25} \cdot (Mg - Mg_{(OBS)})$	µmol Mg cm^{-3} yr^{-1}
R_{26}	$k_{26} \cdot PO_4^{3-}/(PO_4^{3-} + C_{eq}) \cdot NO_{3\,bac}^- \cdot H_2S$	µmol P cm^{-3} yr^{-1}
R_{27}	$k_{27} \cdot P_{poly} \cdot \delta$ where δ =1 for $O_2 \leq 1$ µM and δ =0 for $O_2 > 1$ µM	µmol P cm^{-3} yr^{-1}
R_{28}	$k_{28} \cdot (POC_1 + POC_2) \cdot H_2S$	µmol S cm^{-3} yr^{-1}
R_{29}	$k_{29} \cdot P_{Fish}$	µmol P cm^{-3} yr^{-1}

R_{30}	$k_{30} \cdot H_2 \cdot SO_4^{2-}$	μmol H_2 cm^{-3} yr^{-1}

[a] $\mathrm{RPOC} = \sum_{i=1}^{4} k_{POCi} \cdot \mathrm{POC}_i$; Kinetic limiting terms: $f_{K-j} = \frac{[j]}{[j]+K_j}$, where K_j is the half–saturation constant for species j.

[b] Refers to volume of pore fluid. The factor $\frac{\rho_s \cdot (1-\varphi(x)) \cdot 10^6}{\mathrm{M_W} \cdot \varphi(x)}$ is used to convert between g and μmol cm^{-3} of fluid, where M_W (g mol^{-1}) is the standard atomic weight of the species j in question.

[c] At St. 12, R_{15}, R_{16}, R_{26} and R_{27} were not included since no LSB were observed.

Supplementary Table 7. Modeled depth–integrated turnover rates under steady state conditions.

Rate	St. 12, 23°S	St. 14, 23°S	St. 41, 25°S	Unit
R_1	0.57	0.51	0.94	mmol m^{-2} d^{-1} of C
R_2	1.09	0.50	0.50	mmol m^{-2} d^{-1} of N
R_3	0.20	0.19	0.22	mmol m^{-2} d^{-1} of N
R_4	0.72	0.34	0.094	mmol m^{-2} d^{-1} of Fe
$R_{4P_{Fe}}$	0.042	0.027	0.0066	mmol m^{-2} d^{-1} of P
R_5	3.62	2.52	3.85	mmol m^{-2} d^{-1} of S
R_6	0.013	0.015	0.018	mmol m^{-2} d^{-1} of CH_4
R_7	0.40	0.0042	0.0080	mmol m^{-2} d^{-1} of NO_2^-
R_8	0.044	0.028	0.014	mmol m^{-2} d^{-1} of Fe^{2+}
$R_{8P_{Fe}}$	0.0026	0.0023	0.0010	mmol m^{-2} d^{-1} of P
R_9	0.015	0.015	0.0058	mmol m^{-2} d^{-1} of Fe^{2+}
R_{10}	0.57	4.44×10^{-6}	0.00024	mmol m^{-2} d^{-1} of H_2S
R_{11}	0	0	0	mmol m^{-2} d^{-1} of CH_4
R_{12}	0.37	0.087	0.23	mmol m^{-2} d^{-1} of NH_4^+
R_{13}	0.015	0.082	0.025	mmol m^{-2} d^{-1} of Fe^{2+}
$R_{13P_{Fe}}$	0.00091	0.0070	0.0019	mmol m^{-2} d^{-1} of P
R_{14}	0.67	0.23	0.056	mmol m^{-2} d^{-1} of Fe^{2+}
$R_{14P_{Fe}}$	0.039	0.019	0.0040	mmol m^{-2} d^{-1} of P
R_{15}	-	0.57	1.13	mmol m^{-2} d^{-1} of NO_3^-
R_{16}	-	2.17	3.68	mmol m^{-2} d^{-1} of NO_3^-
R_{17}	0.000	0	0	mmol m^{-2} d^{-1} of NO_3^-
R_{18}	0.89	0.23	0.35	mmol m^{-2} d^{-1} of NH_4^+
R_{19}	0.013	0.015	0.018	mmol m^{-2} d^{-1} of CH_4
R_{20}	0.018	0.016	0.010	mmol m^{-2} d^{-1} of Fe^{2+}
R_{21}	4.41×10^{-4} / 1.87×10^{-2}	4.29×10^{-6} / 2.50×10^{-2}	2.95×10^{-6}/ 1.71×10^{-2}	mmol m^{-2} d^{-1} of H_2S
$R_{21P_{Fe}(HR/MR)}$	2.46×10^{-5} / 1.98×10^{-4}	3.46×10^{-7} / 6.22×10^{-4}	2.1×10^{-7}/ 3.84×10^{-4}	mmol m^{-2} d^{-1} of P
R_{22}	0.0080	0.025	0.015	mmol m^{-2} d^{-1} of Fe^{2+}
$R_{22P_{Fe}}$	0.00025	0.0013	0.00059	mmol m^{-2} d^{-1} of P
R_{23}	0.00104	0.066	0.24	mmol m^{-2} d^{-1} of PO_4^{3-}
R_{24}	0.42	0.051	0.19	mmol m^{-2} d^{-1} of Ca^{2+}
R_{25}	0.050	0.025	0.060	mmol m^{-2} d^{-1} of Mg^{2+}
R_{26}	-	1.83	0.21	mmol m^{-2} d^{-1} of P
R_{27}	-	1.84	0.22	mmol m^{-2} d^{-1} of P
R_{28}	0.0049	0.48	0.36	mmol m^{-2} d^{-1} of S
R_{29}	0.36	0.43	0.33	mmol m^{-2} d^{-1} of P
R_{30}	0.018	0.016	0.010	mmol m^{-2} d^{-1} of H_2
R_{NH_4POC}	1.57	0.79	1.09	mmol m^{-2} d^{-1} of NH_4^+
R_{PO_4POC}	0.031	0.13	0.188	mmol m^{-2} d^{-1} of PO_4^{3-}
R_{POC}	8.72	6.07	9.11	mmol m^{-2} d^{-1} of C

Supplementary Table 8. Modelled fluxes (*F*) at the top (*x*=0) and bottom (*x*=*L*) under steady state conditions. Positive fluxes are directed downwards into the sediment and vice versa.

Flux	St. 12, 23°S		St. 14, 23°S		St. 41, 25°S		Unit
	x=0	*x*=*L*	*x*=0	*x*=*L*	*x*=0	*x*=*L*	
$F_{SO_4^{2-}}$	3.08	0.046	0.60	0.018	0.45	0.033	mmol m^{-2} d^{-1} of SO_4^{2-}
F_{CH_4}	-0.000064	0	-0.000030	0	-0.000050	0	mmol m^{-2} d^{-1} of CH_4
$F_{NH_4^+}$	-0.30	0.0077	-1.02	0.026	-1.64	0.0079	mmol m^{-2} d^{-1} of NH_4^+
F_{DIC}	-8.23	0.020	-5.70	0.28	-8.75	0.088	mmol m^{-2} d^{-1} of DIC
F_{H_2S}	-2.97	0.032	-0.0013	0.072	-0.013	0.021	mmol m^{-2} d^{-1} of H_2S
$F_{PO_4^{3-}}$	-0.39	0.0000060	-0.49	0.00022	-0.28	0.000079	mmol m^{-2} d^{-1} of PO_4^{3-}
$F_{Fe^{2+}}$	-0.00099	0	-0.014	0	-0.0035	0	mmol m^{-2} d^{-1} of Fe^{2+}
F_{O_2}	2.53	0	0.71	0	1.32	0	mmol m^{-2} d^{-1} of O_2
$F_{NO_3^-}$	0.82	0	0.54	0	0.50	0	mmol m^{-2} d^{-1} of NO_3^-
$F_{NO_2^-}$	0.040	0	-0.14	0	-0.14	0	mmol m^{-2} d^{-1} of NO_2^-
F_{TA}	-5.94	0.016	-4.48	0.29	-6.80	0.086	mmol m^{-2} d^{-1} of TA
$F_{Ca^{2+}}$	0.44	0.018	0.081	0.030	0.21	0.019	mmol m^{-2} d^{-1} of Ca^{2+}
$F_{Mg^{2+}}$	0.15	0.096	0.30	0.28	0.20	0.14	mmol m^{-2} d^{-1} of Mg^{2+}
$F_{NO_{3bac}^-}$	-	-	2.75	0	4.82	0	mmol m^{-2} d^{-1} of NO_3^-
F_{H_2}	0	0	0	0	0	0	mmol m^{-2} d^{-1} of H_2
F_{POC_1}	1.25	0	1.49	0	3.29	0	mmol m^{-2} d^{-1} of C
F_{POC_2}	2.49	0	4.48	0	5.76	0	mmol m^{-2} d^{-1} of C
F_{POC_3}	4.99	0	2.98	2.40	0.41	0.0011	mmol m^{-2} d^{-1} of C
F_{POC_4}	8.73	8.73	0	0.48	3.29	3.65	mmol m^{-2} d^{-1} of C
$F_{Fe(OH)_3HR}$	0.0036	0	0.027	0	0.015	0	mmol m^{-2} d^{-1} of Fe
$F_{Fe(OH)_3MR}$	0.011	0	0.000090	0	0.0018	0	mmol m^{-2} d^{-1} of Fe
F_{FeU}	0.16	0.16	0.051	0.051	0.084	0.084	mmol m^{-2} d^{-1} of Fe
$F_{P_{FeHR}}$	0.00014	0	0.0011	0	0.00059	0	mmol m^{-2} d^{-1} of P
$F_{P_{FeMR}}$	0	0	0	0	0	0	mmol m^{-2} d^{-1} of P
$F_{P_{HAp}}$	0	0.0010	0	0.066	0	0.24	mmol m^{-2} d^{-1} of P
F_{FeS_2}	0	0.013	0	0.013	0	0.013	mmol m^{-2} d^{-1} of Fe
$F_{P_{poly}}$	0	0	0	0	0	0	mmol m^{-2} d^{-1} of P
$F_{S_{org}}$	0.51	0.52	0.25	0.73	0.34	0.70	mmol m^{-2} d^{-1} of S
$F_{P_{Fish}}$	0.36	0	0.43	0	0.33	0	mmol m^{-2} d^{-1} of P
$F_{P_{org}}$	0.036	0.0045	0.14	0.0086	0.19	0.0041	mmol m^{-2} d^{-1} of P
$F_{N_{org}}$	2.21	0.64	1.11	0.32	1.53	0.44	mmol m^{-2} d^{-1} of P
Flux ratios							
DIC/PO_4^{3-}	21		12		31		mol C (mol P)$^{-1}$
DIN/PO_4^{3-}	-1.4		1.3		4.6		mol N (mol P)$^{-1}$
$\Sigma NO_3^-/PO_4^{3-}$	-2.1		-1.1		-1.7		mol N (mol P)$^{-1}$
Total $\Sigma NO_3^-/PO_4^{3-}$ [a]	-2.2		-6.4		-18.5		mol N (mol P)$^{-1}$

[a] Also including NO_{3bac}^-

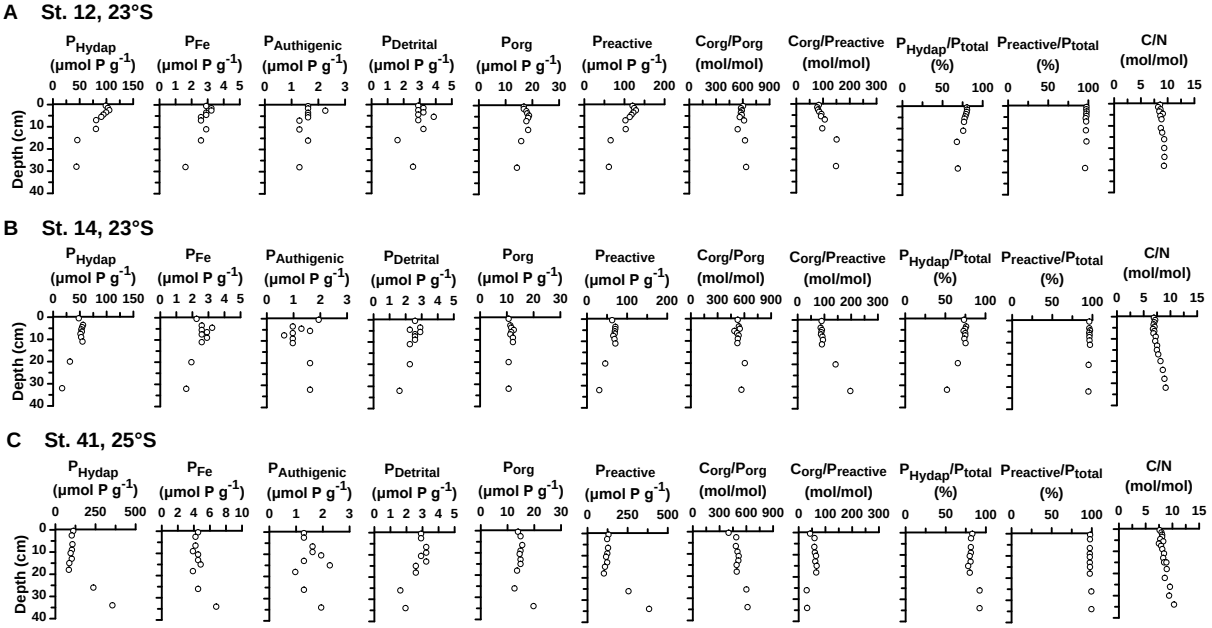

Supplementary Figure 1. Measured depth profiles of P_{Hydap}, P_{Fe}, $P_{Authigenic}$, $P_{Detrital}$, P_{org}, $P_{reactive}$ fractions from sequential extraction ($P_{reactive} = P_{Hydap} + P_{Fe} + P_{Authigenic} + P_{org}$), C_{org}/P_{org} (atomic ratio of POC and P_{org}), $C_{org}/P_{reactive}$ (atomic ratio of POC and $P_{reactive}$), fraction of total P as P_{Hydap}, fraction of total P as $P_{reactive}$ C/N (atomic ratio of POC and TN) at (A) St. 12, (B) St. 14 and (C) St. 41.

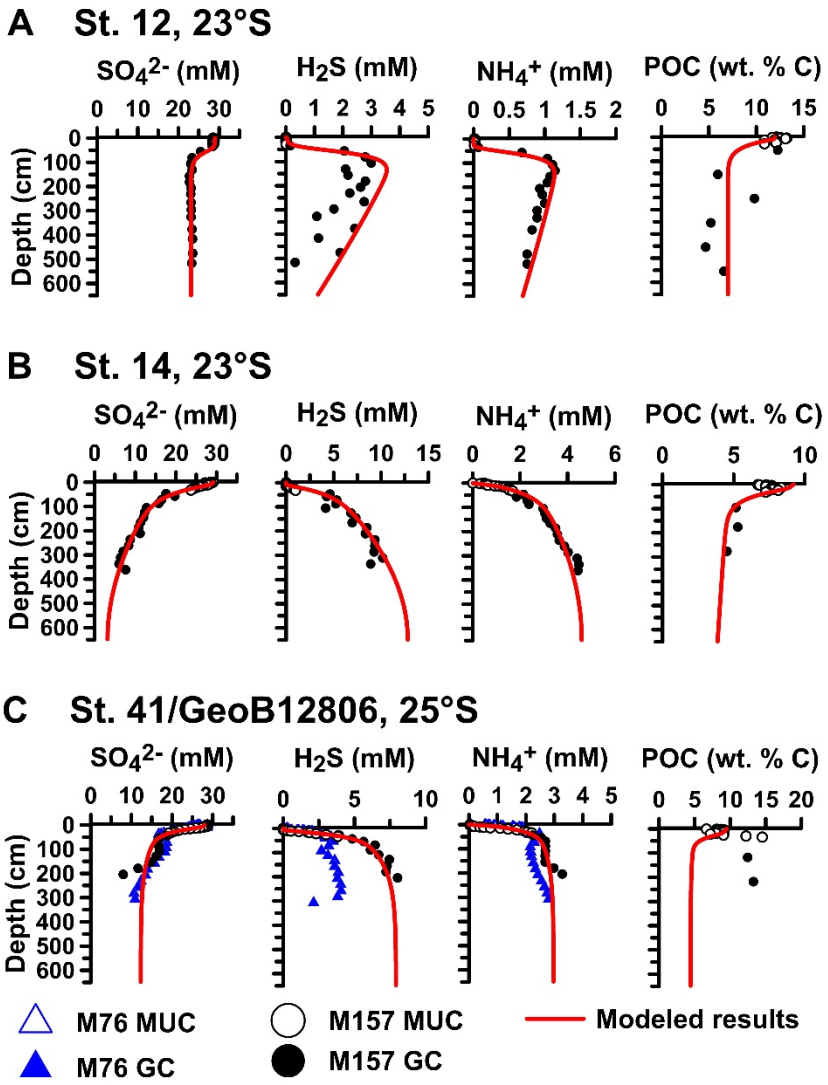

Supplementary Figure 2. Modelled (curves) and measured (symbols) depth profiles of SO_4^{2-}, H_2S and NH_4^+ concentrations and POC contents in the upper 650 cm at (A) St. 12, (B) St. 14 and (C) St. 41 / GeoB12806. The open and closed circles indicate samples collected from cruise M157 cruise and the open and closed triangles represent samples collected from M76.

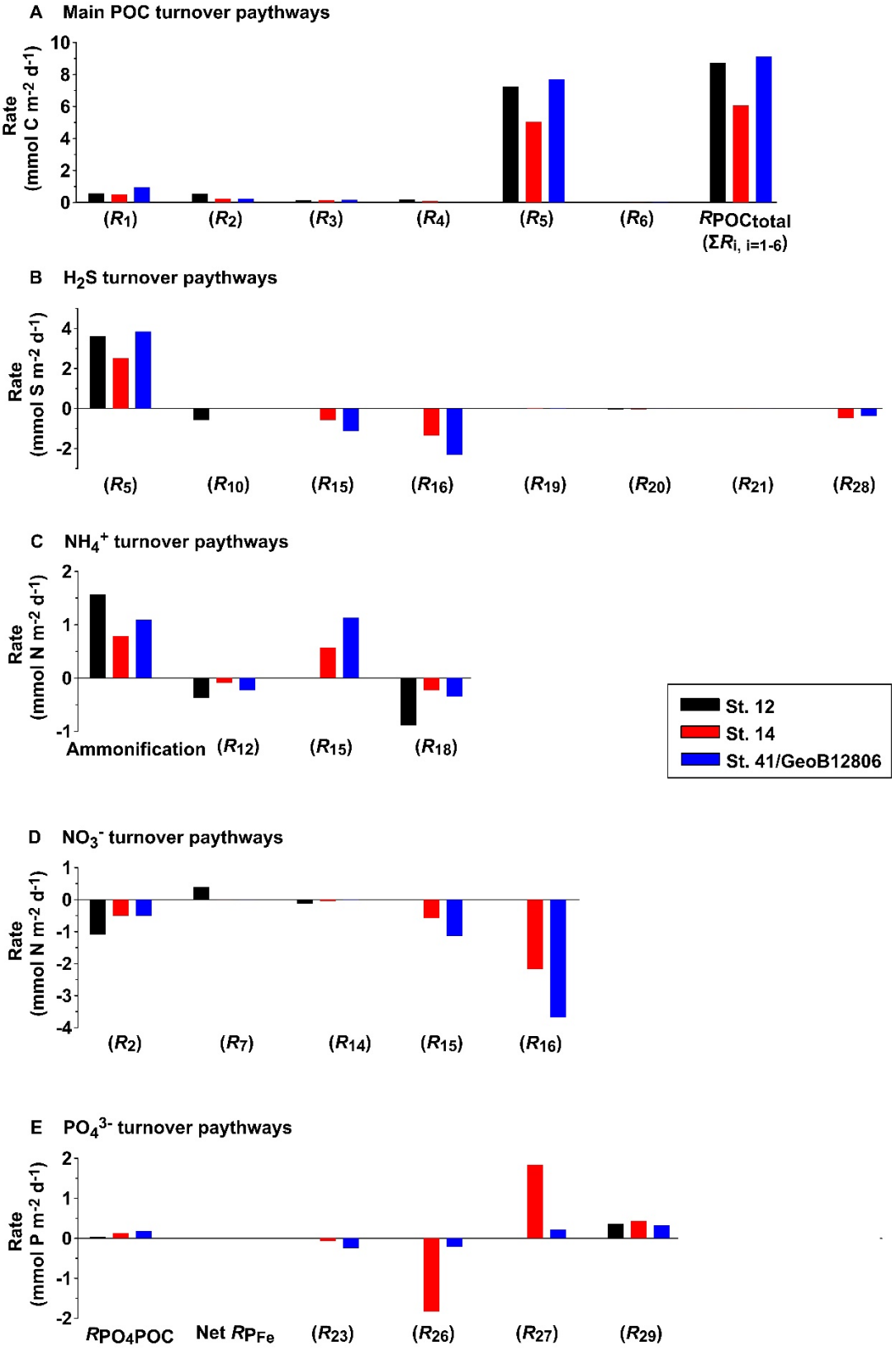

Supplementary Figure 3. Simulated turnover rates of (A) POC, (B) H_2S, (C) NH_4^+, (D) NO_3^- and (E) PO_4^{3-} at the study sites. Reaction numbers are described in Supplementary Table 5. R_{PO4POC} is PO_4^{3-} released from POC degradation, and Net R_{PFe} is the net rate of iron-bound P reactions (R_{4PFe}+R_{8PFe}+R_{13PFe}+R_{14PFe}+R_{21PFe}+R_{22PFe}). Positive numbers in (B) to (E) represent sources and negative numbers represent sinks.

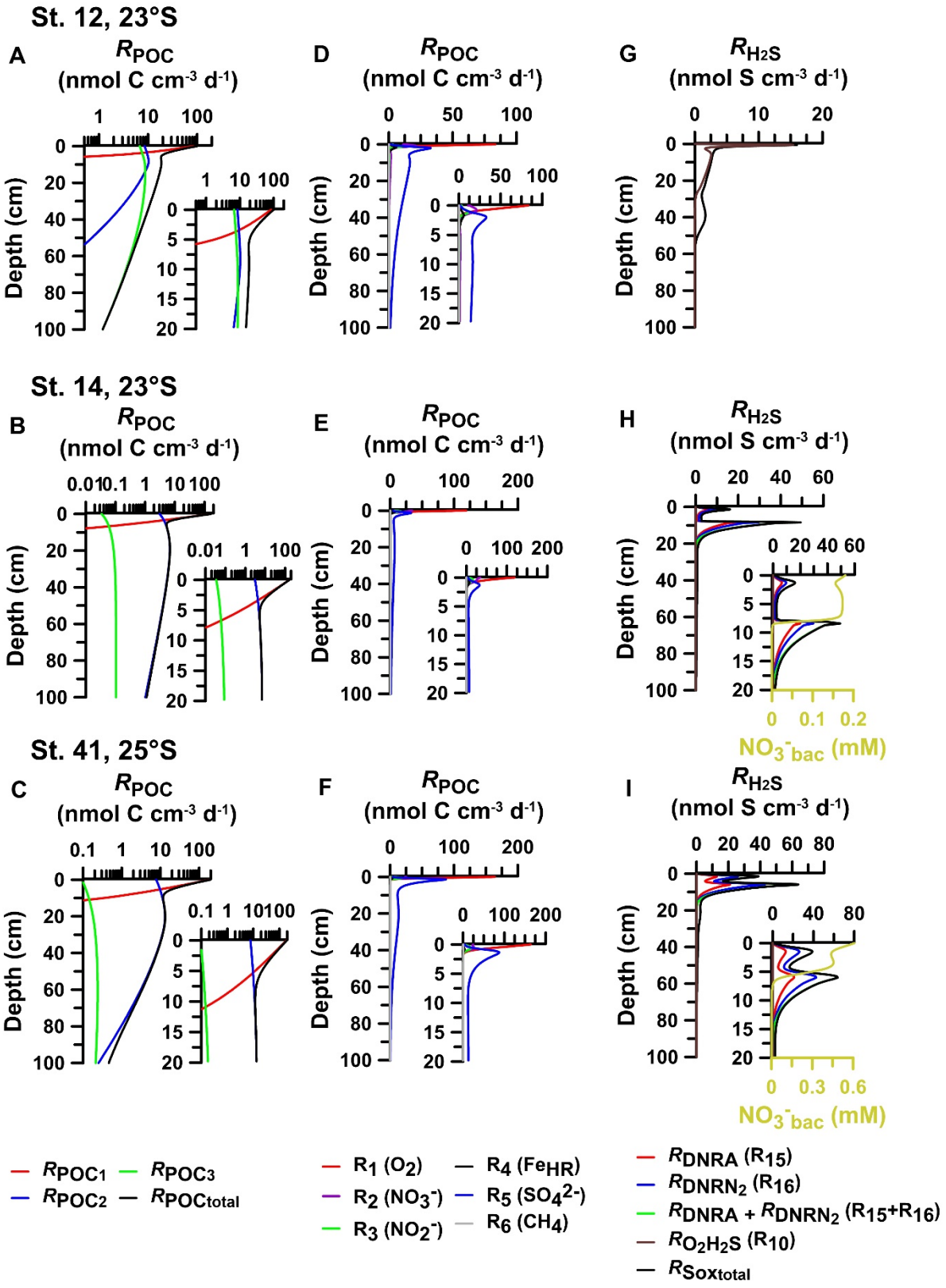

Supplementary Figure 4. Simulated profiles of (A-C) POC degradation rates, (D-F) rates of electron acceptors utilized for POC degradation and (G-I) hydrogen sulfide oxidation rates and $NO_3^-_{bac}$ concentrations in the top 20 cm.

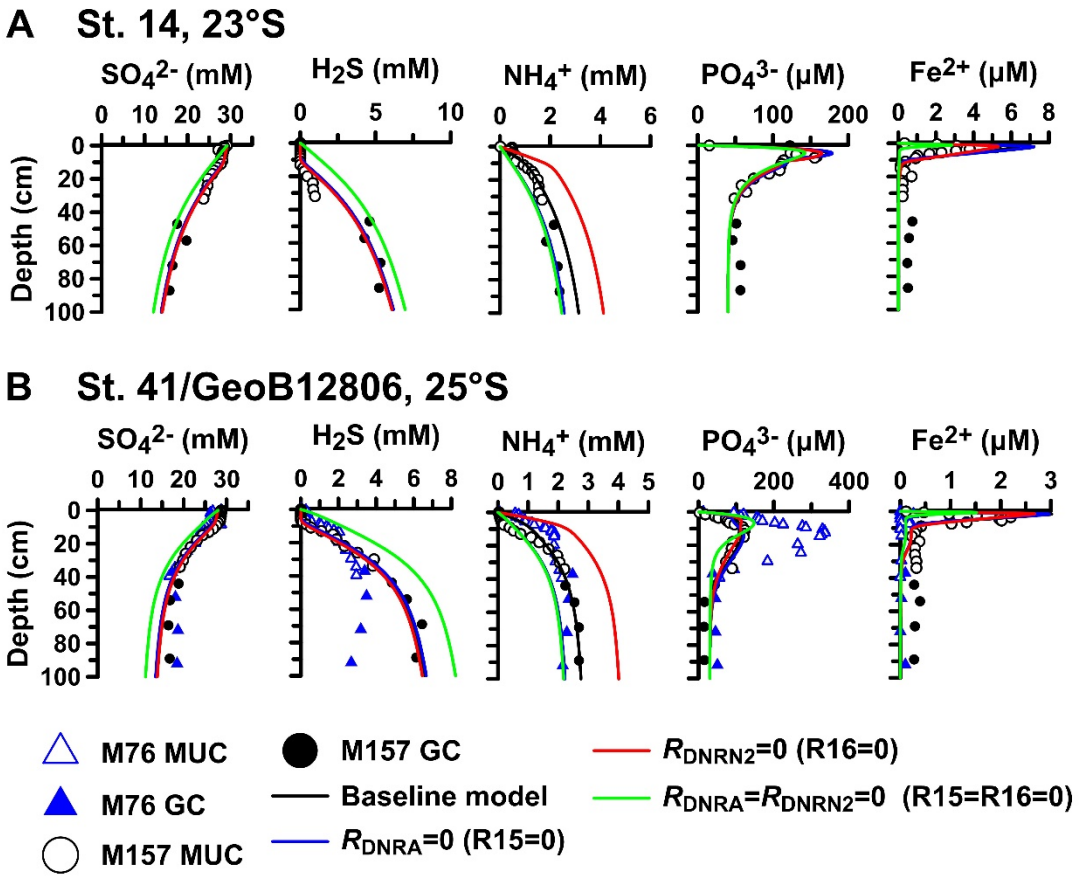

Supplementary Figure 5. Model sensitivity analysis of DNRA (R15) and $DNRN_2$ (R16) at (A) St. 14 and (B) St. 41. Baseline values are shown in black curves and measured data as symbols. The results show that H_2S and NH_4^+ concentrations are sensitive to DNRA and $DNRN_2$.

References

Berner R. A. (1980) Early Diagenesis: A Theoretical Approach. Princeton University Press, Princeton, p. 241.

Bohlen, L., Dale, A.W., Sommer, S., Mosch, T., Hensen, C., Noffke, A., Scholz, F. and Wallmann, K. (2011) Benthic nitrogen cycling traversing the Peruvian oxygen minimum zone. Geochimica et Cosmochimica Acta 75, 6094-6111.

Boudreau B. P. (1997) Diagenetic Models and Their Implementation: Modelling Transport and Reactions in Aquatic Sediments. SpringerVerlag, Berlin, 414p.

Dale, A.W., Bourbonnais, A., Altabet, M., Wallmann, K. and Sommer, S. (2019) Isotopic fingerprints of benthic nitrogen cycling in the Peruvian oxygen minimum zone. Geochimica et Cosmochimica Acta 245, 406-425.

Dale, A.W., Sommer, S., Lomnitz, U., Bourbonnais, A. and Wallmann, K. (2016a) Biological nitrate transport in sediments on the Peruvian margin mitigates benthic sulfide emissions and drives pelagic N loss during stagnation events. Deep Sea Research Part I: Oceanographic Research Papers 112, 123-136.

Dale, A.W., Boyle, R.A., Lenton, T.M., Ingall, E.D. and Wallmann, K. (2016b) A model for microbial phosphorus cycling in bioturbated marine sediments: Significance for phosphorus burial in the early Paleozoic. Geochimica et Cosmochimica Acta 189, 251-268.

Dale, A.W., Brüchert, V., Alperin, M. and Regnier, P. (2009) An integrated sulfur isotope model for Namibian shelf sediments. Geochimica et Cosmochimica Acta 73, 1924-1944.

Zabel, M., Mohrholz, V., Schulz-Vogt, H., Sommer, S. and Zettler, M. (2019) The Benguela System under climate change Effects of variability in physical forcing on carbon and oxygen budgets, Cruise No. M157, 04.08.2019 - 16.09.2019, Mindelo (Cape Verde) - Walvis Bay (Namibia).